Check for updates

Geophysical Research Letters

RESEARCH LETTER
10.1029/2026GL125871

Reaction-Gated Transient Permeability in Ductile Shear Zones

Ioan V. Sanislav[1], Avish Kumar[2], and Mabrouk Sami[3]

[1]Economic Geology Research Centre (EGRU), James Cook University, Townsville, QLD, Australia, [2]Irish Centre for Research in Applied Geosciences (iCRAG), University College Dublin, Dublin, Ireland, [3]Geosciences Department, College of Science, United Arab Emirates University, Al Ain, United Arab Emirates

Key Points:

- A porosity-balance model predicts a sharp permeability switch when connected porosity exceeds a percolation threshold
- Using experimental constraints, creep cavitation alone falls orders of magnitude below this threshold at natural shear-zone strain rates
- A net reaction-driven porosity source can close the gap, making ductile shear-zone permeability transient and reaction-gated

Supporting Information:

Supporting Information may be found in the online version of this article.

Correspondence to:

I. V. Sanislav,
ioan.sanislav@jcu.edu.au

Citation:

Sanislav, I. V., Kumar, A., & Sami, M. (2026). Reaction-gated transient permeability in ductile shear zones. *Geophysical Research Letters*, *53*, e2026GL125871. https://doi.org/10.1029/2026GL125871

Received 30 JUL 2026
Accepted 29 AUG 2026

Author Contributions:

Conceptualization: Ioan V. Sanislav
Formal analysis: Ioan V. Sanislav, Avish Kumar
Investigation: Ioan V. Sanislav
Methodology: Ioan V. Sanislav, Avish Kumar, Mabrouk Sami
Validation: Ioan V. Sanislav
Visualization: Ioan V. Sanislav, Avish Kumar, Mabrouk Sami
Writing – original draft: Ioan V. Sanislav
Writing – review & editing: Avish Kumar, Mabrouk Sami

© 2026 The Author(s). Geophysical Research Letters published by Wiley Periodicals LLC on behalf of American Geophysical Union.
This is an open access article under the terms of the Creative Commons Attribution-NonCommercial License, which permits use, distribution and reproduction in any medium, provided the original work is properly cited and is not used for commercial purposes.

Abstract Ductile shear zones act as transient pathways for crustal fluids, yet the conditions under which their connected porosity becomes sufficient to conduct are not well constrained. We present a porosity balance in which connected porosity evolves under three competing processes: creation by creep cavitation, creation by metamorphic reaction, and thermally activated closure. The model is constrained by existing experimental data, and permeability is linked to porosity through a percolation law with a sharp threshold. Within this constrained model, creep cavitation alone produces a steady-state porosity orders of magnitude below the threshold at natural strain rates. A net reaction-driven porosity source resolves this gap, and the critical net porosity-production rate required to reach the threshold is geologically reasonable. Ductile shear-zone permeability is therefore likely transient and reaction-gated, with deformation alone unable to sustain connectivity at natural rates.

Plain Language Summary Deep in the Earth's crust, rocks deform slowly by flowing rather than breaking, forming narrow zones of intense deformation called shear zones. These zones are important because they can act as channels that allow fluids to move through otherwise impermeable rock—fluids that carry heat, drive chemical reactions, and concentrate metals into ore deposits. But it has not been clear what makes a shear zone open up as a fluid channel, or close again. We build a simple mathematical model that tracks the tiny connected pore spaces in a deforming rock. The model balances processes that create pore space against processes that destroy it, and most of its ingredients are fixed using existing laboratory measurements. The model shows that deformation by itself cannot open enough connected pore space to let fluids through—it falls short by a wide margin. Instead, the pore space needed is supplied by mineral reactions. A shear zone is most likely to conduct fluid when an active reaction supplies connected pore space faster than closure can destroy it.

1. Introduction

Ductile shear zones are sites of strain localization in the middle and lower continental crust, increasingly recognized as transient pathways for metamorphic, magmatic, and hydrothermal fluids (e.g., Fusseis et al., 2009; Menegon & Fagereng, 2021) and as hosts of syn-kinematic fluid flow, mineral precipitation, and metasomatism (e.g., Muñoz-Montecinos & Behr, 2023; Wenning et al., 2018). They also focus the deep hydrothermal fluids responsible for many ore deposits (e.g., Sibson et al., 1988). Yet the same shear zones, once exhumed, are typically of very low permeability (e.g., Wenning et al., 2018). This contrast implies that a ductile shear zone is not a permanent conduit but a structure that transiently opens and closes, and that the connected porosity controlling its permeability is a dynamic quantity, set by a balance between processes that create pore space and processes that destroy it.

The porosity of a deforming rock reflects a competition between dilation and compaction. In creeping aggregates, grain-scale cavitation during viscous flow generates porosity (e.g., Fusseis et al., 2009; Gilgannon et al., 2020), while solution-transfer and viscous closure remove it (e.g., Beeler & Hickman, 2004; Yasuhara et al., 2003). A metamorphic reaction can act as an additional, deformation-independent source or sink of pore space (e.g., Bedford et al., 2017; Schmalholz et al., 2024): dehydration of natural serpentinite generates an interconnected pore network and raises permeability by orders of magnitude, transitorily (Tenthorey & Cox, 2003). Describing when a shear zone conducts fluid therefore requires these competing processes to be assembled into a single porosity balance.

19448007, 2026, 18, Downloaded from https://agupubs.onlinelibrary.wiley.com/doi/10.1029/2026GL125871 by I. V. Sanislav - James Cook University , Wiley Online Library on [28/09/2026]. See the Terms and Conditions (https://onlinelibrary.wiley.com/terms-and-conditions) on Wiley Online Library for rules of use; OA articles are governed by the applicable Creative Commons License

For brittle faults, such a balance already exists: Segall and Rice (1995) described fault-gouge porosity as evolving toward a slip-velocity-dependent steady state, now central to rate-and-state fault models (e.g., Heimisson et al., 2021). That framework is restricted to frictional granular deformation, and no equivalent exists for viscous shear zones. The granular fluid pump of Fusseis et al. (2009) provides the closest conceptual model for the viscous regime, in which creep cavitation generates a transient, deforming pore network and grain-scale pressure gradients drive fluid through it. That model operates at the grain scale and describes active pumping through a network taken to be poorly connected, whereas the balance developed here operates at the shear-zone scale and asks whether bulk connected porosity crosses the percolation threshold. The two are complementary. Numerical models based on continuum damage mechanics have separately treated creep-driven void growth and strain localisation in deforming crust (Karrech et al., 2012). A complete test of the granular fluid pump would additionally require the energetic stationary state of the shear zone to be modeled (Fusseis et al., 2009; Hobbs et al., 2011). The bulk balance represents these couplings in aggregated form, complementing the fully coupled thermodynamic-mechanical-chemical description called for by Gilgannon et al. (2021).

This is important, because permeability does not increase smoothly with porosity. In low-porosity rocks it is controlled by pore-network connectivity and rises sharply only once porosity exceeds a percolation threshold (e.g., Bernabé et al., 2003; Peach & Spiers, 1996). Percolation theory has been applied to crustal shear zones (O'Hara, 1994), and microtomographic analysis confirms that mylonite pore networks percolate only above a threshold porosity (Liu & Regenauer-Lieb, 2011). A shear zone therefore behaves as a switch, sealing below the threshold and conducting above it. Determining whether it is a conduit or a seal reduces to whether its connected porosity can be driven across this threshold, and held there, against the processes that close it.

These ingredients exist independently in the literature (Fusseis et al., 2009; O'Hara, 1994; Schmalholz et al., 2024; Segall & Rice, 1995; Tenthorey & Cox, 2003), but no compact, experimentally constrained porosity balance combines creep cavitation, reaction-driven connected-porosity production, thermally activated closure, and a percolation threshold, and derives a critical reaction rate for permeability activation. We present such a balance, transferring the brittle rate-and-state porosity-evolution approach to the viscous regime with creep cavitation as the deformation source, and adding reaction and closure terms. The model is deliberately a bulk, phenomenological description that tracks volume-averaged connected porosity and does not resolve individual pores, grain-scale cavity growth, or local fluid-pressure fluctuations. It describes advective flow through a percolating pore network and does not treat mass transfer by intracrystalline or solid-state diffusion, which can move fluid components without a connected pore network. Three of the four terms are constrained from existing data. We use the constrained model to ask whether creep cavitation at natural strain rates can raise connected porosity to the percolation threshold, and find that it cannot, by a wide margin. The shortfall requires a reaction-driven source, at rates consistent with independently determined metamorphic reaction rates.

2. An Experimentally Constrained Porosity Balance

2.1. Governing Equation

We describe the connected porosity φ of a ductile shear zone as a single quantity that evolves in time under three competing processes. Following the porosity-evolution approach introduced for brittle faults by Segall and Rice (1995), in which gouge porosity relaxes toward a velocity-dependent steady state, we write a balance in which deformation and reaction add connected pore space while a thermally activated process removes it:

$$\frac{d\varphi}{dt} = (A\dot{\gamma} + S_{\mathrm{rxn}})\left(1 - \frac{\varphi}{\varphi_*}\right) - B\varphi \tag{1}$$

Here $\dot{\gamma}$ is the shear strain-rate magnitude, A is a dimensionless cavitation efficiency, S_{rxn} is the net reaction-driven porosity source rate, and B is a temperature-dependent closure rate. The deformation term $A\dot{\gamma}$ represents porosity generated by grain-scale creep cavitation during viscous flow (Fusseis et al., 2009; Gilgannon et al., 2020); the reaction term S_{rxn} represents net porosity produced by a solid-volume-reducing reaction (Bedford et al., 2017; Schmalholz et al., 2024); and $B\varphi$ represents closure by solution-transfer and viscous processes (Beeler & Hickman, 2004; Yasuhara et al., 2003). The factor $(1 - \varphi/\varphi^*)$ limits the source terms as connected porosity approaches φ^*, the source-saturation porosity at which the porosity-producing terms vanish, so the steady state itself lies below φ^*, operationally identified with the porosity at which measured permeability saturates or rolls

19448007, 2026, 18, Downloaded from https://agupubs.onlinelibrary.wiley.com/doi/10.1029/2026GL125871 by I. V. Sanislav - James Cook University , Wiley Online Library on [28/09/2026]. See the Terms and Conditions (https://onlinelibrary.wiley.com/terms-and-conditions) on Wiley Online Library for rules of use; OA articles are governed by the applicable Creative Commons License

over. φ^* is constrained by the same experiments that define the permeability law (Section 2.2): the permeability of synthetic salt saturates and declines above $\varphi \approx 1.5\%$ (Peach & Spiers, 1996), and that of calcite–quartz aggregates above $\varphi \approx 5\%$–8% (Xiao et al., 2006). S_{rxn} is the net rate at which reaction progress creates connected pore volume after accounting for connectivity and precipitation (see Supporting Information S1); unlike the cavitation source, it is not assumed to scale directly with the instantaneous bulk strain rate. Throughout, φ denotes the bulk, volume-averaged network-forming pore-volume fraction, a proxy for the pore space available to form a hydraulically connected network. Local porosity in a mylonite is heterogeneous, and large syn-kinematic pores in porphyroclast strain shadows (Fusseis et al., 2023) can locally exceed the bulk value.

For constant temperature, strain rate, and reaction source, Equation 1 has a steady state,

$$\varphi_{ss} = \frac{(A\dot{\gamma} + S_{rxn})\varphi_*}{(A\dot{\gamma} + S_{rxn}) + B\varphi_*} \tag{2}$$

toward which porosity relaxes. The steady-state porosity is set by the combined source rate, the closure rate, and the saturation porosity φ^*. Whether a shear zone conducts fluid depends on whether φ_{ss} lies above or below the percolation threshold φ_c.

2.2. The Permeability Switch

Permeability is related to connected porosity by a percolation power law,

$$k = K(\varphi - \varphi_c)^n \tag{3}$$

which applies for $\varphi > \varphi_c$, with a small background permeability k_0 below threshold; permeability does not literally vanish at φ_c but drops to k_0, the matrix permeability of the host rock. Figure 1 shows this relationship for two independent rock systems. Synthetic salt deformed in shear (Peach & Spiers, 1996) defines the law over the range $\varphi \approx 0.1\%$–3%; a least-squares fit to the rising limb ($\varphi < 1.3\%$) gives $\varphi_c = 0.084\%$ (95% confidence interval 0.03%–0.19%) and $n = 1.26$ (0.7–1.9). Hot-pressed calcite–quartz aggregates (Xiao et al., 2006) define the same form of relationship in a silicate-bearing rock, with a percolation threshold of 4%–6%. The threshold value is system-dependent, because it is governed by pore geometry rather than by mineralogy; the common and robust feature of both data sets is the existence of a sharp threshold below which the rock is effectively impermeable. A shear zone is thus a permeability switch: connected porosity below φ_c leaves it sealing, and connected porosity above φ_c allows it to conduct. The percolation law adopted here treats connected porosity as a bulk, isotropic quantity. In natural mylonites the pore network is anisotropic and is commonly organized into periodic pore sheets (Gilgannon et al., 2021), and the experimental data sets used to constrain the threshold derive from lower-strain, approximately isotropic deformation. The threshold values are therefore bulk, order-of-magnitude estimates rather than exact transfers to the high-strain, anisotropic case. The percolation law also equates network connectivity with hydraulic connectivity. Where fluid wetting is poor the dihedral angle can leave a geometrically connected network hydraulically discontinuous, and reported dihedral angles for mid-crustal fluid-mineral systems are commonly high enough for fluid to remain poorly connected, varying with fluid composition and pressure (Holness, 1992; Watson & Brenan, 1987).

2.3. The Closure Term

The closure rate B is constrained by experiment. Pore space in a fluid-saturated rock is removed by solution-transfer at a rate that is, thermally activated, so B follows an Arrhenius form, $B = B_0 \exp(-E/RT)$. Figure 2a compiles closure-rate estimates from two independent sources: pressure-solution closure rates derived from quartz experiments (Beeler & Hickman, 2004; Yasuhara et al., 2003), and permeability-reduction rates measured directly in quartz gouge (Giger et al., 2007). A least-squares Arrhenius fit through all estimates gives an activation energy of 69 kJ mol^{-1}, consistent with the activation energy of quartz dissolution. The estimates scatter by a factor of approximately 14, so B is constrained only to order-of-magnitude precision and is shown in Figure 2a as a band. Closure rates span $B \approx 10^{-11}$ s^{-1} at 75°C to $B \approx 10^{-4}$ s^{-1} at 500°C.

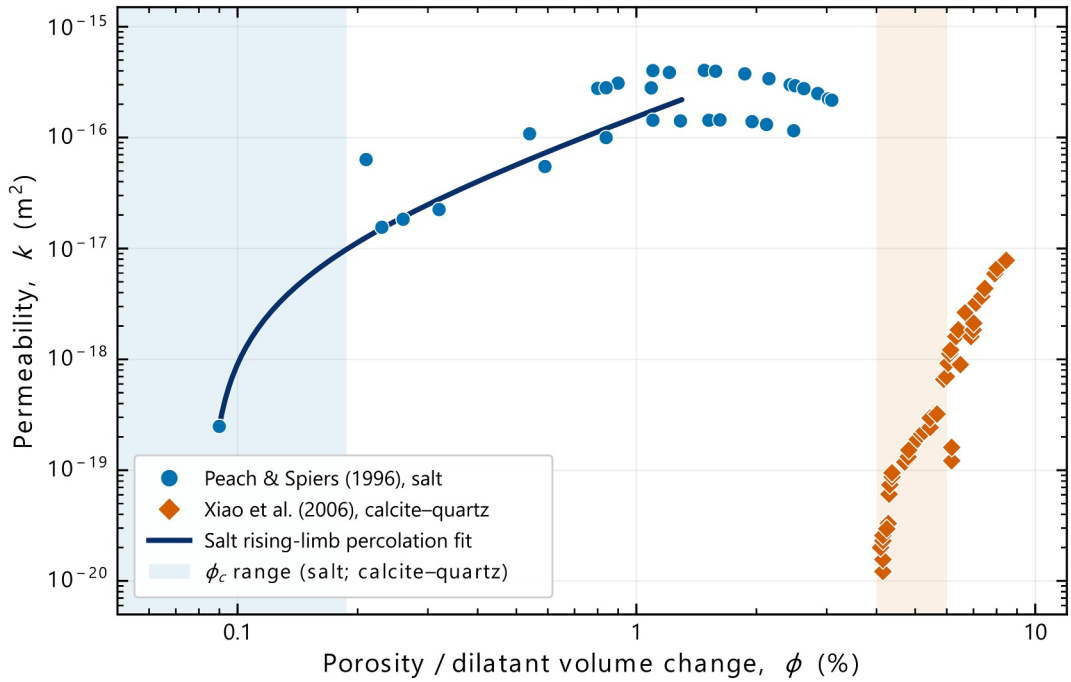


Figure 1. The horizontal axis represents porosity or deformation-induced dilatant volume change, used as a proxy for connected pore volume rather than as a direct measurement of model φ. Blue circles: synthetic salt deformed in shear (Peach & Spiers, 1996, p. 32 measurements). Solid curve: salt rising-limb percolation fit $k = K(\varphi - \varphi_c)^n$ to the rising limb ($\varphi < 1.3\%$), with $\varphi_c = 0.084\%$ (95% confidence interval 0.03%–0.19%), $n = 1.26$ (0.7–1.9), and $K = 5.67 \times 10^{-14}$ m^2. The salt data plateau and decline above $\varphi \approx 1.5\%$ (permeability saturation); this rollover defines the saturation porosity $\varphi*$, and the fit is not applied beyond the rising limb. Orange diamonds: hot-pressed calcite–quartz aggregates (Xiao et al., 2006; 41 values digitised from their Figure 12, three quartz contents pooled). Shaded vertical bands mark percolation threshold ranges: 0.03%–0.19% for salt (blue) and 4%–6% for calcite–quartz (orange). Both systems show a sharp, percolation-controlled permeability rise at a material-dependent threshold.

2.4. The Deformation Term

The deformation-driven source $A\dot{\gamma}$ is bounded by experiment. Torsion experiments on calcite aggregates, in which creep cavitation generates connected porosity during high-strain viscous flow (Gilgannon et al., 2020, 2021), provide a laboratory-scale, order-of-magnitude estimate of the ratio A/B at approximately 6 s. Gilgannon and co-workers measure pore-sheet porosity and strain rate but not A, B, or steady-state porosity directly, so A/B is lab-inferred rather than calibrated, a favorable estimate of the cavitation-to-closure timescale A/B. A/B is calibrated on carbonate (Carrara marble) deformation and is expected to depend on mineralogy, deformation mechanism, grain size, and fluid chemistry, so it is treated here as an order-of-magnitude hypothesis rather than a universal constraint for mid- and lower-crustal shear zones. As shown in Section 3, even allowing an order-of-magnitude uncertainty, the cavitation-supported porosity remains four to six orders below the threshold, so the conclusion does not depend on a precise A/B.

2.5. The Reaction Term

The reaction source S_{rxn} is the one term in Equation 1 that cannot be reduced to a single calibrated value. We restrict it to a net porosity-producing source, folding net-sealing reactions into the closure term B. Reaction rates are specific to the reaction, temperature, and fluid, and span a wide range, so we bracket S_{rxn} rather than calibrate it. At the fast end, gypsum-dehydration experiments produce connected porosity at rates of order 10^{-5} s^{-1} (Bedford et al., 2017). At the slow end, field-based regional reaction rates are four to seven orders slower than laboratory predictions, giving reaction-progress rates of order 10^{-15}–10^{-13} s^{-1} (Baxter, 2003), which bound the connected-porosity source from above. Natural reaction rates are comparable to, and bounded above by, the bulk strain rates of the same rocks (Baxter & DePaolo, 2004). The reaction term therefore spans 8 to 10 orders of magnitude, carried through as a bracketed range. The bracket also treats the reaction source as independent of

19448007, 2026, 18, Downloaded from https://agupubs.onlinelibrary.wiley.com/doi/10.1029/2026GL125871 by I. V. Sanislav - James Cook University , Wiley Online Library on [28/09/2026]. See the Terms and Conditions (https://onlinelibrary.wiley.com/terms-and-conditions) on Wiley Online Library for rules of use; OA articles are governed by the applicable Creative Commons License

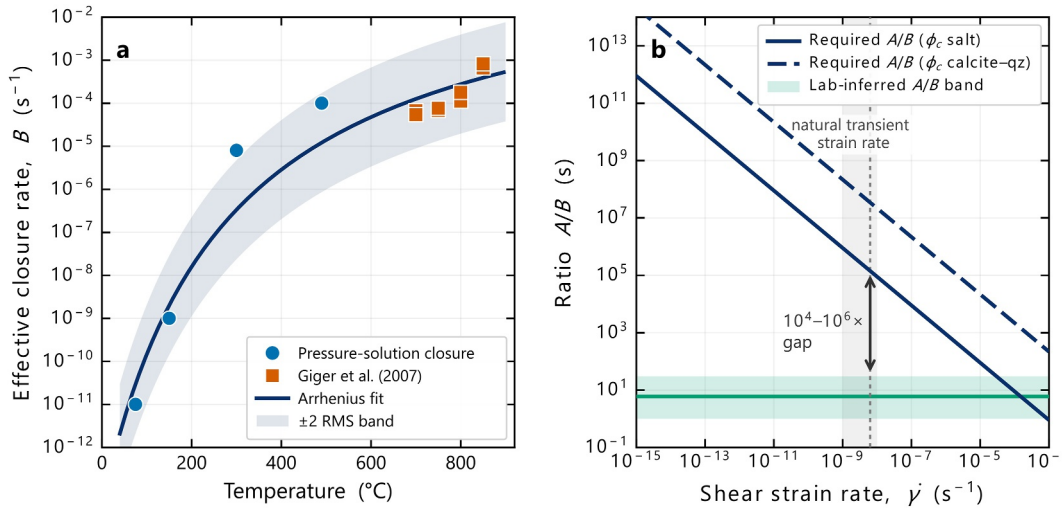


Figure 2. (a) Effective pore-closure rate B as a function of temperature; the plotted estimates combine pressure-solution closure rates and permeability-decay rates. Circles: pressure-solution experiments on quartz (Beeler & Hickman, 2004; Yasuhara et al., 2003). Squares: permeability-reduction rates in quartz gouge (Giger et al., 2007). Solid line: least-squares Arrhenius fit (activation energy 69 kJ mol^{-1}); shaded band: ±2 RMS scatter (a factor of approximately 14), reflecting that B is constrained only to order-of-magnitude precision. (b) The rate paradox. Curves: A/B required for cavitation-driven steady-state porosity to reach φ_c in the $\varphi*-$ limited model, as a function of shear strain rate, for the salt threshold (solid) and the calcite–quartz threshold (dashed). Green band: lab-inferred A/B (Gilgannon et al., 2021), as an order-of-magnitude band. Vertical gray band: natural transient shear-zone strain rate (Campbell & Menegon, 2019).

fluid pressure, whereas fluid pressure can exert the dominant control on reaction rate (Llana-Fúnez et al., 2012) and thus on the porosity-production rate, a feedback the fixed range does not capture. Three of the four terms are thus constrained by existing data; only S_{rxn} remains a range.

3. The Paradox

3.1. Cavitation-Only Steady State

Three of the four terms in Equation 1 are constrained by experiment. We now ask whether deformation alone, creep cavitation with no reaction source, can drive a shear zone across the percolation threshold. Setting $S_{rxn} = 0$ in Equation 2, the steady-state porosity supported by cavitation is

$$\varphi_{ss} = \frac{A\dot{\gamma}\varphi_*}{A\dot{\gamma} + B\varphi_*} \tag{4}$$

For φ_{ss} well below the saturation porosity $\varphi*$, this reduces to $\varphi_{ss} \approx (A/B)\cdot\dot{\gamma}$. The cavitation-only steady-state porosity is therefore the product of the experimentally constrained ratio A/B and the shear strain rate. Because A/B is adopted as approximately 6 s from the torsion experiments (Section 2.4), φ_{ss} is determined entirely by the strain rate at which the shear zone deforms.

3.2. The Strain-Rate Gap

Natural ductile shear zones deform far more slowly than laboratory samples. Shear zones accommodate strain in transient pulses at rates of order 10^{-8}–10^{-9} s^{-1} (Campbell & Menegon, 2019), with lower long-term background rates. At a representative transient rate of 6×10^{-9} s^{-1}, the cavitation-only steady state is $\varphi_{ss} \approx 4 \times 10^{-8}$. This is four to six orders of magnitude below the percolation thresholds determined in Figure 1—0.084% for salt and 4%–6% for calcite–quartz.

The shortfall can be expressed as a requirement on A/B. For φ_{ss} to reach the percolation threshold φ_{ss}, the ratio A/B must be at least $\varphi_c\varphi*/\left[\dot{\gamma}(\varphi* - \varphi_c)\right]$. Figure 2b shows this required ratio as a function of strain rate, together with the lab-inferred value. At the natural transient rate, reaching the salt threshold would require $A/B \approx 1 \times 10^5$ s,

19448007, 2026, 18, Downloaded from https://agupubs.onlinelibrary.wiley.com/doi/10.1029/2026GL125871 by I. V. Sanislav - James Cook University , Wiley Online Library on [28/09/2026]. See the Terms and Conditions (https://onlinelibrary.wiley.com/terms-and-conditions) on Wiley Online Library for rules of use; OA articles are governed by the applicable Creative Commons License

and reaching the calcite–quartz threshold would require $A/B \approx 3 \times 10^7$ s—four to six orders of magnitude larger than the lab-inferred value of order 6 s. No plausible cavitation efficiency closes this gap: even an order-of-magnitude larger A would leave the shear zone far below threshold.

3.3. Why Cavitation Is Unlikely to Compensate by Slowing Closure

One might expect the gap to close at depth, but higher temperatures accelerate closure (Figure 2a) and, unless A rises in proportion, lower the realised A/B, making threshold crossing less likely rather than more. Although A may vary with temperature, recrystallization, grain size, fluid chemistry, and deformation mechanism, existing data show no orders-of-magnitude increase in A/B sufficient to close the gap (Section 3.2).

This is the central result of the constrained model. Under the experimentally inferred A/B range, extrapolated to natural strain rates, a ductile shear zone deforming by creep cavitation alone is unlikely to raise its connected porosity to the percolation threshold. The transient permeability that ductile shear zones are observed to possess (Section 1) must be supplied by a process that does not depend on strain rate in the same way. Creep cavitation is associated with grain-size-sensitive creep and viscous grain-boundary sliding (Passchier & Trouw, 2005), whereas some natural shear zones deform dominantly by dislocation creep. The cavitation-only steady state is therefore a hypothetical upper bound on the deformation-supplied porosity, and where dislocation creep dominates, cavitation is not the operative source, reinforcing the need for a reaction-driven source.

4. The Resolution

4.1. A Reaction-Supported Steady State

The paradox of Section 3 arises because the cavitation source scales with strain rate, and natural strain rates are low. A reaction source need not scale with the instantaneous bulk strain rate. Metamorphic reactions proceed at rates set by temperature, fluid availability, and reaction affinity (Baxter, 2003). Where a reaction is coupled to deformation through dissolution-precipitation creep, its rate is bounded above by the bulk strain rate (Baxter & DePaolo, 2004). Externally driven reactions such as prograde dehydration are not paced by deformation and can supply porosity independently of strain rate. With the reaction term S_{rxn} retained, the steady-state porosity is given by Equation 2. Because S_{rxn} is independent of $\dot{\gamma}$, it sets a floor on φ_{ss} that persists even as the strain rate tends to zero: in the limit $A\dot{\gamma} \ll S_{\mathrm{rxn}}$, the steady state reduces to $\varphi_{ss} \approx S_{\mathrm{rxn}}\varphi*/(S_{\mathrm{rxn}} + B\varphi*)$, a quantity controlled entirely by the competition between reaction and closure.

Figure 3 shows steady-state porosity as a function of strain rate at mid-crustal temperature, for cavitation alone and for a series of reaction rates spanning the bracketed range of Section 2.5. The cavitation-only curve falls steeply with decreasing strain rate and lies far below the percolation threshold at natural rates (Section 3). Each reaction curve, by contrast, is flat at low strain rate, holding porosity at a fixed floor that rises with S_{rxn}: for $S_{\mathrm{rxn}} \gtrsim 10^{-9}$ s^{-1} the floor approaches or exceeds the salt percolation threshold, while reaching the higher calcite–quartz threshold requires S_{rxn} closer to 10^{-6} s^{-1}. A reaction in the upper part of the bracketed range therefore lets a shear zone conduct at strain rates where cavitation alone leaves it sealed.

4.2. The Critical Reaction Rate

The resolution can be made quantitative. Setting the steady-state porosity of Equation 2 equal to the percolation threshold φ_{c} and solving for the reaction rate gives the critical reaction rate $S_{\mathrm{rxn},c}$ required to switch a shear zone on:

$$S_{\mathrm{rxn,c}} = \max\left[0, \frac{B\varphi_c\varphi_*}{\varphi_* - \varphi_c} - A\dot{\gamma}\right] \tag{5}$$

The max(0, ⋯) form makes explicit that $S_{\mathrm{rxn},c}$ vanishes if cavitation alone already supplies the threshold porosity $\left(A\dot{\gamma} \geq B\varphi_{\mathrm{c}}\varphi*/\left(\varphi* - \varphi_{\mathrm{c}}\right)\right)$; at the natural strain rates considered here this condition is not satisfied and $S_{\mathrm{rxn,c}}$ is strictly positive. The expression also requires $\varphi_{\mathrm{c}} < \varphi*$: as φ_{c} approaches $\varphi*$ the required reaction source diverges, and if $\varphi_{\mathrm{c}} \geq \varphi*$ the pore network cannot reach percolation within this model. For calcite–quartz, where

19448007, 2026, 18, Downloaded from https://agupubs.onlinelibrary.wiley.com/doi/10.1029/2026GL125871 by I. V. Sanislav - James Cook University , Wiley Online Library on [28/09/2026]. See the Terms and Conditions (https://onlinelibrary.wiley.com/terms-and-conditions) on Wiley Online Library for rules of use; OA articles are governed by the applicable Creative Commons License

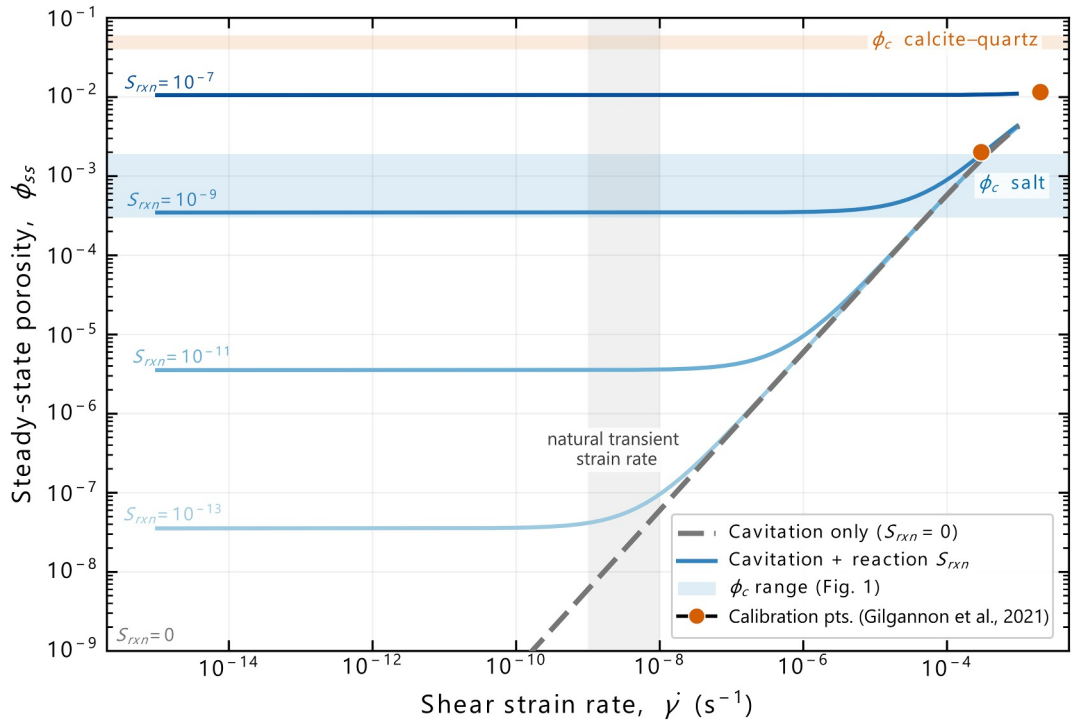


Figure 3. Steady-state porosity φ_{ss} as a function of shear strain rate, computed from the $\varphi*-$ limited porosity balance at mid-crustal temperature (closure rate B from Figure 2; lab-inferred $A/B = 6$ s from Gilgannon et al., 2021). Dashed gray curve: cavitation only ($S_{\mathrm{rxn}} = 0$); at the natural transient strain-rate band (vertical gray shading; Campbell & Menegon, 2019) it lies far below both percolation threshold bands φ_c (horizontal shading: salt in blue, calcite–quartz in orange, from Figure 1). Blue curves: steady state with a strain-rate-independent reaction source term $S_{\mathrm{rxn}} = 10^{-13}$ to 10^{-7} s^{-1}. Because S_{rxn} does not depend on strain rate, it sets a porosity floor that is, independent of deformation rate; $S_{\mathrm{rxn}} \approx 10^{-9}$ s^{-1} approaches the lower (salt) percolation threshold, and S_{rxn} closer to 10^{-6} s^{-1} is needed to exceed the higher calcite–quartz threshold. Orange circles: calibration points used to constrain A/B (Gilgannon et al., 2021).

$\varphi_c \approx 4\%–6\%$ and $\varphi* \approx 5\%–8\%$ lie close together, $S_{\mathrm{rxn},c}$ is sensitive to $\varphi*$ and the model is correspondingly less constraining for that system.

At steady state, a shear zone conducts fluid when S_{rxn} exceeds $S_{\mathrm{rxn,c}}$ and is sealed when S_{rxn} falls below it, whereas the instantaneous state responds to a change in source rate with a finite lag. The critical rate depends only on quantities already constrained: the closure rate B, the percolation threshold φ_c and saturation porosity $\varphi*$ from Figure 1, and the deformation term $A\dot{\gamma}$. At the natural transient strain rate and mid-crustal temperature, $S_{\mathrm{rxn,c}}$ is approximately 3×10^{-9} s^{-1} for the salt percolation threshold and 6×10^{-7} s^{-1} for the higher calcite–quartz threshold. Both values lie within the reaction-rate range of Section 2.5 (Baxter, 2003; Bedford et al., 2017). The salt value lies just below the natural strain rate, but the net source is the reaction rate reduced by the reaction's solid-volume change and by the connectivity of the porosity it produces, so reaching even the salt threshold with a strain-paced reaction requires efficient conversion to connected porosity, and a less efficient reaction must outpace bulk strain. The calcite–quartz value exceeds the natural strain rate by about two orders of magnitude and requires a reaction not paced by bulk strain: externally driven dehydration (Bedford et al., 2017) or reaction that generates its own local overpressure and stress (Plümper et al., 2022). Higher-threshold silicate systems therefore switch on only where reaction is locally vigorous or strain-decoupled, whereas the lower-threshold case is more permissive but still contingent on reaction efficiency.

4.3. Consistency With Observations

This prediction is consistent with several independent lines of evidence. Creep cavitation is well documented (Fusseis et al., 2009; Gilgannon et al., 2020), but the cavities produced in experiments are transient and poorly connected, real but insufficient on their own. The serpentinite dehydration experiments of Tenthorey and Cox (2003), in which permeability rose by at least three orders of magnitude during reaction and was transitory,

19448007, 2026, 18, Downloaded from https://agupubs.onlinelibrary.wiley.com/doi/10.1029/2026GL125871 by I. V. Sanislav - James Cook University , Wiley Online Library on [28/09/2026]. See the Terms and Conditions (https://onlinelibrary.wiley.com/terms-and-conditions) on Wiley Online Library for rules of use; OA articles are governed by the applicable Creative Commons License

19448007, 2026, 18, Downloaded from https://agupubs.onlinelibrary.wiley.com/doi/10.1029/2026GL125871 by I. V. Sanislav - James Cook University , Wiley Online Library on [28/09/2026]. See the Terms and Conditions (https://onlinelibrary.wiley.com/terms-and-conditions) on Wiley Online Library for rules of use; OA articles are governed by the applicable Creative Commons License

are a direct analogue of the behavior predicted here. Where natural shear zones show syn-kinematic fluid flow, that flow is repeatedly associated with metamorphic reaction rather than deformation alone (Bedford et al., 2017; Schmalholz et al., 2024). The coincidence of reaction and fluid migration in mylonites (Muñoz-Montecinos & Behr, 2023; Wenning et al., 2018) is, in this framework, not incidental: reaction carries the porosity budget across the percolation threshold, so fluid flow is expected where reaction is active.

4.4. Implications for the Permeability of Shear Zones

Two consequences follow. First, the permeability of a ductile shear zone is likely reaction-gated: a slowly deforming shear zone hosting an active, net porosity-producing reaction may conduct fluid, while a fast-deforming but unreactive one is predicted to remain sealed. Second, the conduit is intrinsically transient because the reaction source is finite in duration: while a net porosity-producing reaction is active it can hold connected porosity above threshold, and once the source declines, closure returns the system toward the sub-threshold cavitation-only state. The steady-state criterion (Equation 5) is necessary but not sufficient for a finite episode, which must also exceed the critical rate and persist longer than the threshold-crossing time, and the conduit can remain open briefly after reaction ends. The shear zone therefore conducts only while reaction sustains connectivity, matching the episodic conduit behavior these structures are inferred to show (Muñoz-Montecinos & Behr, 2023; Wenning et al., 2018).

5. Implications and Conclusions

The model resolves whether a ductile shear zone conducts fluid into a competition between three rates: porosity creation by deformation, creation by reaction, and thermally activated closure. Two conclusions follow for reading shear-zone permeability from the rock record.

First, within this constrained model the synkinematic permeability of a ductile shear zone is decoupled from that of the same rock once exhumed. The conduit is sustained while reaction supplies connected porosity faster than closure removes it. Once reaction ends, closure drives porosity back below threshold, leaving a low residual porosity that records the sealed state. This is consistent with field observations: lower-crustal shear zones preserve only small synkinematic porosities (Menegon et al., 2015), and retrograde shear zones of low present-day permeability nonetheless record abundant fluid presence during deformation (Stenvall et al., 2020). The permeability of an exhumed mylonite is therefore a lower bound on its synkinematic value, and paleo-fluid-flux estimates from preserved porosity will systematically underestimate the throughput permitted while active.

Second, because reaction supplies a porosity floor that does not scale with strain rate, the timing of fluid flow is tied to the timing of metamorphic reaction. Fluid flow is therefore predicted to be episodic, each episode coupled to a reaction and set by its lifetime. This bulk-scale timing criterion is complementary to the grain-scale granular fluid pump of Fusseis et al. (2009): the pump operates while viscous grain-boundary sliding is active, whereas the criterion here identifies reaction as holding porosity above threshold.

Many ore deposits form where hydrothermal fluids are focused along crustal structures (Blenkinsop et al., 2020; Cox, 2005; Sanislav et al., 2023; Sibson et al., 1988). The transient, reaction-gated permeability described here provides a mechanism by which deep crustal structures can episodically deliver large fluid volumes while leaving little permeability preserved in the rock record.

The model makes a testable prediction: where a ductile shear zone preserves evidence of synkinematic fluid flow, that flow should coincide in space and time with an active metamorphic reaction, and intervals of deformation without a net porosity-producing reaction are not expected to have sustained bulk percolating permeability at these strain rates. S_{rxn} is the one term we bracket rather than calibrate. Direct measurement of its porosity-production rate for specific reactions would calibrate it.

Conflict of Interest

The authors declare no conflicts of interest relevant to this study.

Availability Statement

No new data were generated for this study. All data used are from previously published sources, listed here and compiled with their values in Supporting Information S1. Permeability–porosity data are from Peach and Spiers (1996) for synthetic salt and Xiao et al. (2006) for calcite–quartz aggregates. Pore-closure-rate data are from Yasuhara et al. (2003), Beeler and Hickman (2004), and Giger et al. (2007). Cavitation-porosity and strain-rate data used to constrain *A*/*B* are from Gilgannon et al. (2020, 2021). Reaction and porosity-production-rate data are from Tenthorey and Cox (2003), Bedford et al. (2017), Baxter (2003), Baxter and DePaolo (2004), and Schmalholz et al. (2024). Natural shear-zone strain-rate and fluid-pressure data are from Campbell and Menegon (2019) and Menegon and Fagereng (2021).

Acknowledgments
The first author would like to acknowledge funding from the Resources Technology and Critical Mineral Trailblazer (10821) and the continuous support received from the Economic Geology Research Centre (EGRU). Open access publishing facilitated by James Cook University, as part of the Wiley - James Cook University agreement via the Council of Australasian University Librarians.

References

Baxter, E. F. (2003). *Natural constraints on metamorphic reaction rates* (Vol. 220, pp. 183–202). Geological Society, London, Special Publications. https://doi.org/10.1144/gsl.sp.2003.220.01.11

Baxter, E. F., & DePaolo, D. J. (2004). Can metamorphic reactions proceed faster than bulk strain? *Contributions to Mineralogy and Petrology*, *146*(6), 657–670. https://doi.org/10.1007/s00410-003-0525-3

Bedford, J., Fusseis, F., Leclère, H., Wheeler, J., & Faulkner, D. (2017). A 4D view on the evolution of metamorphic dehydration reactions. *Scientific Reports*, *7*(1), 6881. https://doi.org/10.1038/s41598-017-07160-5

Beeler, N. M., & Hickman, S. H. (2004). Stress-induced, time-dependent fracture closure at hydrothermal conditions. *Journal of Geophysical Research*, *109*(B2), B02211. https://doi.org/10.1029/2002jb001782

Bernabé, Y., Mok, U., & Evans, B. (2003). Permeability-porosity relationships in rocks subjected to various evolution processes. *Pure and Applied Geophysics*, *160*(5–6), 937–960. https://doi.org/10.1007/pl00012574

Blenkinsop, T. G., Oliver, N. H. S., Dirks, P. H. G. M., Nugus, M., Tripp, G., & Sanislav, I. (2020). Structural geology applied to the evaluation of hydrothermal gold deposits. In J. V. Rowland, & D. A. Rhys (Eds.), *Applied structural geology of ore-forming hydrothermal systems*.

Campbell, L. R., & Menegon, L. (2019). Transient high strain rate during localized viscous creep in the dry lower continental crust (Lofoten, Norway). *Journal of Geophysical Research: Solid Earth*, *124*(10), 10240–10260. https://doi.org/10.1029/2019jb018052

Cox, S. F. (2005). Coupling between deformation, fluid pressures, and fluid flow in ore-producing hydrothermal systems at depth in the crust. In J. W. Hedenquist, J. F. H. Thompson, R. J. Goldfarb, & J. P. Richards (Eds.), *Economic Geology One Hundredth Anniversary Volume* (pp. 39–75). Society of Economic Geologists. https://doi.org/10.5382/av100.04

Fusseis, F., Allsop, C., Gilgannon, J., Schrank, C., Harley, S., & Schlepütz, C. M. (2023). Strain shadow "megapores" in mid-crustal ultramylonites. *Geology*, *51*(8), 748–752. https://doi.org/10.1130/g51128.1

Fusseis, F., Regenauer-Lieb, K., Liu, J., Hough, R. M., & De Carlo, F. (2009). Creep cavitation can establish a dynamic granular fluid pump in ductile shear zones. *Nature*, *459*(7249), 974–977. https://doi.org/10.1038/nature08051

Giger, S. B., Tenthorey, E., Cox, S. F., & Fitz Gerald, J. D. (2007). Permeability evolution in quartz fault gouges under hydrothermal conditions. *Journal of Geophysical Research*, *112*(B7), B07202. https://doi.org/10.1029/2006jb004828

Gilgannon, J., Poulet, T., Berger, A., Barnhoorn, A., & Herwegh, M. (2020). Dynamic recrystallization can produce porosity in shear zones. *Geophysical Research Letters*, *47*(7), e2019GL086172. https://doi.org/10.1029/2019gl086172

Gilgannon, J., Waldvogel, M., Poulet, T., Fusseis, F., Berger, A., Barnhoorn, A., & Herwegh, M. (2021). Experimental evidence that viscous shear zones generate periodic pore sheets. *Solid Earth*, *12*(2), 405–420. https://doi.org/10.5194/se-12-405-2021

Heimisson, E. R., Rudnicki, J., & Lapusta, N. (2021). Dilatancy and compaction of a rate-and-state fault in a poroelastic medium: Linearized stability analysis. *Journal of Geophysical Research: Solid Earth*, *126*(8), e2021JB022071. https://doi.org/10.1029/2021jb022071

Hobbs, B. E., Ord, A., & Regenauer-Lieb, K. (2011). The thermodynamics of deformed metamorphic rocks: A review. *Journal of Structural Geology*, *33*(5), 758–818. https://doi.org/10.1016/j.jsg.2011.01.013

Holness, M. B. (1992). Equilibrium dihedral angles in the system quartz–CO_2–H_2O–NaCl at 800°C and 1–15 kbar: The effects of pressure and fluid composition on the permeability of quartzites. *Earth and Planetary Science Letters*, *114*(1), 171–184. https://doi.org/10.1016/0012-821x(92)90159-s

Karrech, A., Poulet, T., & Regenauer-Lieb, K. (2012). A limit analysis approach to derive a thermodynamic damage potential for non-linear geomaterials. *Philosophical Magazine*, *92*(28–30), 3439–3450. https://doi.org/10.1080/14786435.2012.687469

Liu, J., & Regenauer-Lieb, K. (2011). Application of percolation theory to microtomography of structured media: Percolation threshold, critical exponents, and upscaling. *Physical Review E*, *83*(1), 016106. https://doi.org/10.1103/physreve.83.016106

Llana-Fúnez, S., Wheeler, J., & Faulkner, D. R. (2012). Metamorphic reaction rate controlled by fluid pressure not confining pressure: Implications of dehydration experiments with gypsum. *Contributions to Mineralogy and Petrology*, *164*(1), 69–79. https://doi.org/10.1007/s00410-012-0726-8

Menegon, L., & Fagereng, Å. (2021). Tectonic pressure gradients during viscous creep drive fluid flow and brittle failure at the base of the seismogenic zone. *Geology*, *49*(10), 1255–1259. https://doi.org/10.1130/g49012.1

Menegon, L., Fusseis, F., Stünitz, H., & Xiao, X. (2015). Creep cavitation bands control porosity and fluid flow in lower crustal shear zones. *Geology*, *43*(3), 227–230. https://doi.org/10.1130/g36307.1

Muñoz-Montecinos, J., & Behr, W. M. (2023). Transient permeability of a deep-seated subduction interface shear zone. *Geophysical Research Letters*, *50*(20), e2023GL104244. https://doi.org/10.1029/2023gl104244

O'Hara, K. D. (1994). Fluid-rock interaction in crustal shear zones: A directed percolation approach. *Geology*, *22*(9), 843–846. https://doi.org/10.1130/0091-7613(1994)022<0843:friics>2.3.co;2

Passchier, C. W., & Trouw, R. A. J. (2005). *Microtectonics* (2nd ed.). Springer.

Peach, C. J., & Spiers, C. J. (1996). Influence of crystal plastic deformation on dilatancy and permeability development in synthetic salt rock. *Tectonophysics*, *256*(1–4), 101–128. https://doi.org/10.1016/0040-1951(95)00170-0

Plümper, O., Wallis, D., Teuling, F., Moulas, E., Schmalholz, S. M., Amiri, H., & Müller, T. (2022). High-magnitude stresses induced by mineral-hydration reactions. *Geology*, *50*(12), 1351–1355. https://doi.org/10.1130/g50493.1

Sanislav, I. V., Mathur, R., Rea, P., Dirks, P. H. G. M., Mahan, B., Godfrey, L., & Degeling, H. (2023). A magmatic copper and fluid source for the sediment-hosted Mount Isa deposit. *Geochemical Perspectives Letters*, *27*, 26–31. https://doi.org/10.7185/geochemlet.2330

19448007, 2026, 18, Downloaded from https://agupubs.onlinelibrary.wiley.com/doi/10.1029/2026GL125871 by I. V. Sanislav - James Cook University , Wiley Online Library on [28/09/2026]. See the Terms and Conditions (https://onlinelibrary.wiley.com/terms-and-conditions) on Wiley Online Library for rules of use; OA articles are governed by the applicable Creative Commons License

Schmalholz, S. M., Khakimova, L., Podladchikov, Y., Bras, E., Yamato, P., & John, T. (2024). (De)hydration front propagation into zero-permeability rock. *Geochemistry, Geophysics, Geosystems*, *25*(9), e2023GC011422. https://doi.org/10.1029/2023gc011422

Segall, P., & Rice, J. R. (1995). Dilatancy, compaction, and slip instability of a fluid-infiltrated fault. *Journal of Geophysical Research*, *100*(B11), 22155–22171. https://doi.org/10.1029/95jb02403

Sibson, R. H., Robert, F., & Poulsen, K. H. (1988). High-angle reverse faults, fluid-pressure cycling, and mesothermal gold-quartz deposits. *Geology*, *16*(6), 551–555. https://doi.org/10.1130/0091-7613(1988)016<0551:harffp>2.3.co;2

Stenvall, C. A., Fagereng, Å., Diener, J. F. A., & Janney, P. E. (2020). Sources and effects of fluids in continental retrograde shear zones: Insights from the Kuckaus Mylonite Zone, Namibia. *Geofluids*, *2020*, 3023268. https://doi.org/10.1155/2020/3023268

Tenthorey, E., & Cox, S. F. (2003). Reaction-enhanced permeability during serpentinite dehydration. *Geology*, *31*(10), 921–924. https://doi.org/10.1130/g19724.1

Watson, E. B., & Brenan, J. M. (1987). Fluids in the lithosphere, 1. Experimentally-determined wetting characteristics of CO_2–H_2O fluids and their implications for fluid transport, host-rock physical properties, and fluid inclusion formation. *Earth and Planetary Science Letters*, *85*(4), 497–515. https://doi.org/10.1016/0012-821x(87)90144-0

Wenning, Q. C., Madonna, C., de Haller, A., & Burg, J.-P. (2018). Permeability and seismic velocity anisotropy across a ductile–brittle fault zone in crystalline rock. *Solid Earth*, *9*(3), 683–698. https://doi.org/10.5194/se-9-683-2018

Xiao, X., Evans, B., & Bernabé, Y. (2006). Permeability evolution during non-linear viscous creep of calcite rocks. *Pure and Applied Geophysics*, *163*, 2071–2102.

Yasuhara, H., Elsworth, D., & Polak, A. (2003). A mechanistic model for compaction of granular aggregates moderated by pressure solution. *Journal of Geophysical Research*, *108*(B11), 2530. https://doi.org/10.1029/2003jb002536

References From the Supporting Information

Dove, P. M., & Crerar, D. A. (1990). Kinetics of quartz dissolution in electrolyte solutions using a hydrothermal mixed flow reactor. *Geochimica et Cosmochimica Acta*, *54*(4), 955–969. https://doi.org/10.1016/0016-7037(90)90431-j

Rimstidt, J. D., & Barnes, H. L. (1980). The kinetics of silica-water reactions. *Geochimica et Cosmochimica Acta*, *44*(11), 1683–1699. https://doi.org/10.1016/0016-7037(80)90220-3

19448007, 2026, 18, Downloaded from https://agupubs.onlinelibrary.wiley.com/doi/10.1029/2026GL125871 by I. V. Sanislav - James Cook University , Wiley Online Library on [28/09/2026]. See the Terms and Conditions (https://onlinelibrary.wiley.com/terms-and-conditions) on Wiley Online Library for rules of use; OA articles are governed by the applicable Creative Commons License